OBJECT ORIENTED FINITE ELEMENT MODELLING AND FRACTURE ANALYSIS OF EPOXY-CLAY NANOCOMPOSITE

A

DISSERTATION

Submitted in partial fulfilment of the requirement
for the award of degree of

MASTER OF ENGINEERING

IN

CAD/CAM ENGINEERING

Submitted

by

Yogeshwar Jasra

(Roll No. 801281025)

Under Supervision of

Mr. Bikramjit Sharma
Assistant Professor
Mechanical Engineering Department

MECHANICAL ENGINEERINGDEPARTMENT
THAPAR UNIVERSITY
PATIALA-147004, PUNJAB
JULY 2014

CERTIFICATE

I hereby declare that the thesis entitled "**Object Orientiented Finite Element Modeling And Fracture Analysis Of Epoxy-Clay Nanocomposite**" is an authentic record of my study carried out as requirements for the award of the degree of **Master of Engineering** in **CAD/CAM Engineering** at **Thapar University, Patiala** under the supervision of **Mr. Bikramjit Sharma**, Assistant Professor, Mechanical Engineering Department, Thapar University, Patiala during July, 2012 to July, 2014. The matter embodied in this report has not been submitted in partial or full to any other university or institute for the award of any degree.

Date: 17/07/2014

Yogeshwar Jasra

It is certified that the above statement made by the student is correct to the best of my/our knowledge and belief.

Bikramjit Sharma 17/7/14

Mr. Bikramjit Sharma
Mechanical Engineering Department
Thapar University, Patiala - 147004

Countersigned by

Dr. Ajay Batish
Professor & Head
Mechanical Engineering Department

Dr. S.K. Mohapatra
Dean of Academic Affairs
Thapar University, Patiala - 147004

ACKNOWLEDGEMENTS

I express my sincere gratitude to my guide **Mr. Biramjit Sharma**, Assistant Professor Mechanical Engineering Department, Thapar University, Patiala, for his invaluable guidance, proper advice and constant encouragement during the course of my work in this dissertation.

I would also express my gratitude to **Dr. Ajay Batish**, Head, Mechanical Engineering Department for his inspirational guidance and whole hearted corporation which helped me to present this dissertation.

I thank the entire faculty and staff of Mechanical Engineering Department, Thapar University, for their help and moral support.

YOGESHWAR JASRA

ABSTRACT

Nanocomposites contains highly variable and irregular angular structure of fillers. This work describes numerical modelling of epoxy-clay nanocomposites based on the real mapping of nano/microstructures. The fundamental material characterisation was conducted using scanning electron microscopy (SEM). To model exact morphology of epoxy-clay nanocomposite, computational models were established by implementing an innovative object-oriented finite element analysis code (OOF). The mechanical and thermal properties of nanocomposites calculated by OOF was in good agreement with the theoretical models. The propagation of cracks, stress and displacement distribution in epoxy-clay nanocomposite is also studied by Abaqus Extended Finite Element (XFEM).

TABLE OF CONTENTS

LIST OF TABLES

LIST OF FIGURES

ABBREVIATIONS

OOFEM	Object Oriented Finite Element method
SEM	Scanning Electron Microscopy
NIST	National Institute of Standards and Technology
XFEM	Extended Finite Element Method
FEM	Finite Element Method
OOF2	Object Oriented Finite Element Analysis version 2
MRF	Modulus Reduction Factor
ROM	Rule of Mixtures
IROM	Inverse Rule of Mixtures

NOTATIONS

E	Energy
α	Inverse aspect ratio
E_{hom}	Homogeneous Energy
E_{shape}	Shape Energy
E_C	Elastic modulus of composite
E_m	Elastic modulus of matrix
E_f	Elastic modulus of filler
ϕ_f	Volume fraction
ζ	Shape parameter
l	Length
d	Diameter
t	Thickness
υ	Poisson ratio
MPa	Mega Pascal
GPa	Giga Pascal

CHAPTER 1

INTRODUCTION

1.1 INTRODUCTION TO COMPOSITE MATERIAL

During the last decades, there has been as remarkable increase in the utilization of composite materials in various fields of application such as sporting goods, structural components for the automotive and aerospace industries. Composites have exceptional mechanical properties combined with a low weight in order to ensure safety. Composite material is the combination two or more constituent materials, which have different chemical and physical properties, and after combination produce a material with different characteristics. Composites can be tailored to achieve low weight, high temperature performance, high stiffness, high Strength, high hardness, conductivity and good corrosion resistance.

The most familiar example of the composite material is concrete which is composed of loose stones in the matrix of cement. Concrete is a very strong material, much stronger than cement, and will not fail until under quite a large force. It can resist high forces, reinforced with concrete and give ability to resist against tensile loading [18].

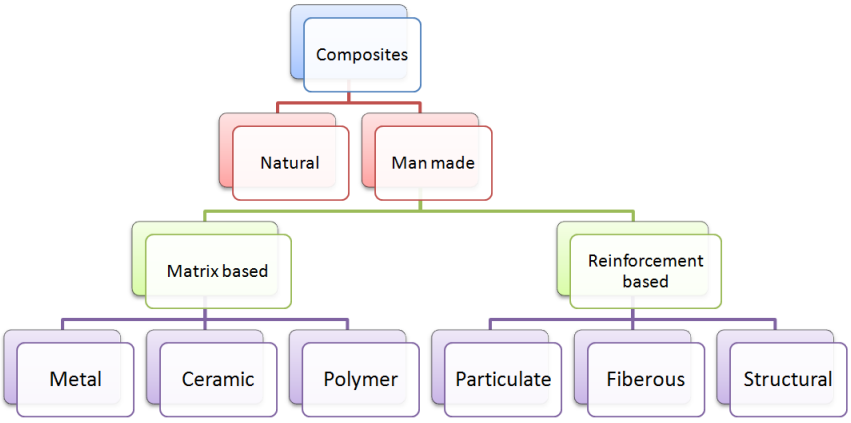

Figure 1.1: Classification of composites material [26]

1.1.1 Matrix phase

The improved properties of the composite materials is due to the reinforcement, but the role of matrix can not be neglected as it hold up the reinforcements and help them in carrying loads. The matrix material not only binds the reinforcements but also improve firmness of the composite material. Selection of matrix is based on the type of application for which it is used for example matrix should be thermodynamically stable for the use for high temperature applications. Material such as aluminium and magnesium alloys due to low density and high thermal conductivity widely used as matrix [19].

The matrix material can be classified as:

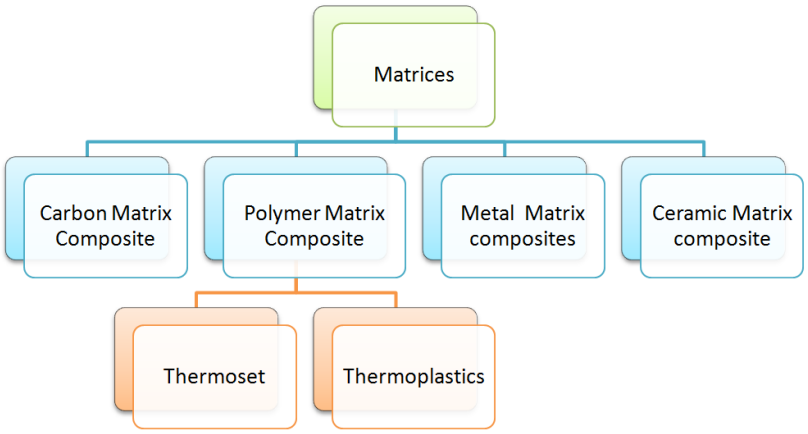

Figure 1.2: Classification of matrix material [26]

1.1.2 Reinforcement phase

A tough fibrous material when included into the primary phase to improve its mechanical properties called reinforcements. Typical examples of reinforcements are carbon, fibers, graphite and metal glass. The main difference between the filler and reinforcement is that fillers do not improves the mechanical properties whereas reinforcement improves tensile and flexural strength [19]. Reinforcements used in composites can be fabrics, whiskers or fibers. Particles reinforcements do not have any preferred orientation and shape. The different types of reinforcements is shown in the figure.1.3.

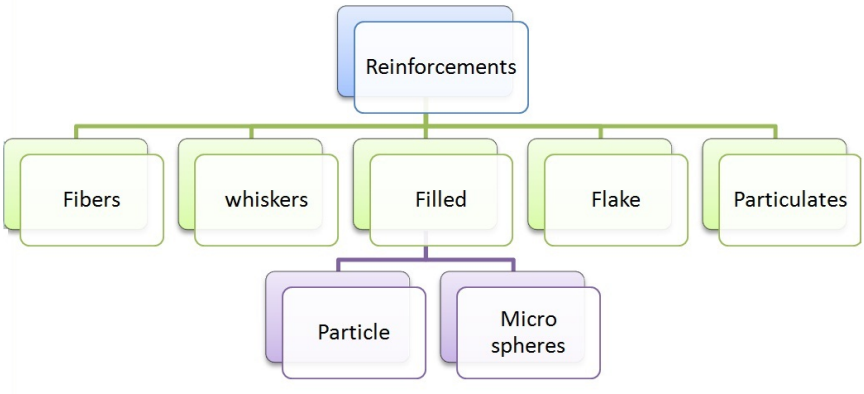

Figure 1.3: Types of reinforcement [33]

1.2 NANOCOMPOSITES

When dimensions at one of the constituent of a composite is less than 100 nanometers (nm) then it is called nanocomposite. The mechanical, electrical, thermal, optical, electrochemical properties of the nanocomposite is different from the phase component. Shells and bones are natural occurring nanocomposites. The nanocomposites are different from the traditional composites due to the exceptionally small size of the reinforcing phase and they have high aspect ratio.

1.2.1 Epoxy nanocomposites

The first industrially-produced epoxy resin was introduced to market in 1946. The applications of epoxy resin includes: coating, electrical, automotive, marine, aerospace and civil infrastructure as well as tool fabrication and pipes and vessels in the chemical industry. In the aerospace industry, epoxy-composites material can be found in various part of the body and structure of military and civil aircrafts, with the number of applications on the rise. The term 'epoxy resin' refers to the polymer and its cured resin/hardener system. The former is a low molecular weight oligomer that contains one or more epoxy groups per molecule (more than one unit per molecule is required if the resultant material is to be cross-linked). Epoxy resins can be cross-linked through a polymerization reaction with a hardener at room temperature or at elevated temperature. Curing agents are used for room temperature cure are usually aliphatic amines, whilst commonly used higher temperature, higher performance hardener are aromatic amines and acid anhydrides [20].

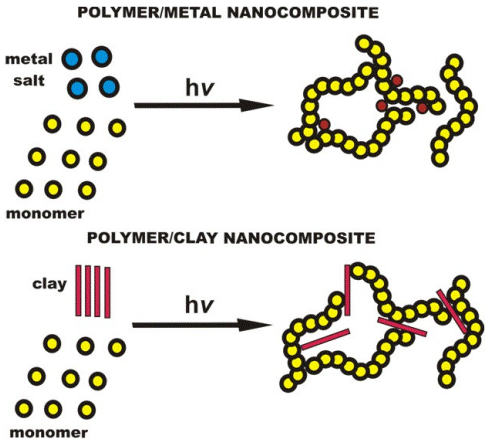

Figure 1.4: Polymer clay nanocomposite [34]

Clay as nanoparticles such as clays are incorporated into polymers to form resulting polymer nanocomposites, which may possess unique electrical, mechanical and optical properties. The clay as filler is expected to strengthen the mechanical properties even upon lower loading of filler. Fiber retardancy, barrier resistance and ion conductivity are expected to be influenced by loading of clay as filler. Polymer/clay nanocomposites comprise organic/inorganic hybrid polymer matrices containing platelet-shaped clay particles that have sizes of the order of a few nanometers thick and several hundred nanometers long. Partly because of their aspect ratios and high surface areas, the clay particles, if properly dispersed in the polymer matrix at a loading level of 1 to 5 wt %, impart unique combinations of chemical properties and physical that makes these nanocomposites attractive for making films and coatings for a variety of industrial applications. Relative to the unmodified polymer, the polymer/clay nanocomposites may exhibit improvements in strength, modulus, and toughness, tear, radiation, fire resistance, and lower thermal expansion and permeability to gases while retaining a high degree of optical transparency. The most common type of nanoclay is montmorillonite (MMT), Clay minerals such as talc and mica that have been used as fillers for years.

1.2.2 Applications of nanocomposites

Highly scratch resistant coating containing nano fillers: When nanoparticles such as Al2O3, SiO2, ZrO2 and TiO2 are reinforced into matrix significantly enhance the scratch resistance. Ceramic nanoparticles have been found as appropriate hardening materials to significantly improve clearcoat hardness and therefore scratch resistance [20].

Nano-coatings with anti-corrosion performance for car bodies: Anti-corrosive coatings both are used to protect metal body against corrosive materials. The most important of these coatings are Cr(VI) due to its excellent anti-corrosion performance has been widely used to protect car bodies from corrosive environment. The high anti-corrosion performance of this coating is related to its high self-healing behavior in corrosive environment.

High-strength steels for car bodies: In order to enhance cars and passengers safety at crashes, the automotive producers have attempted to use high-strength steels in car bodies. A multifunctional protective coating produced based on nanotechnological approach with the principles of conventional paint technologies which significantly increases the strength of steels.

Nanostructured tyres: Silica and organosilane are the important examples of materials used to enhance rubber properties. Adding such materials to rubber composition at nanometric dimensions can significantly improve tyre properties. The size and surface modification of the particles can affect their physical interactions with rubber matrix. Nano sized particles can significantly enhance tyre durability as well as higher fuel efficiency.

Antimicrobial/antibacterial and anti-odour properties of automobile fabric: Textiles can grant an appropriate environment for micro-organisms growth especially at proper humidity and temperature in contact to human body. Various anti-microbial agents such as oxidising agents, diphenyl ether (bis-phenyl) derivatives, ammonium compounds and chitosan have been used. Application of many of Oxidising agents has been avoided because of their harmful or toxic effects. More recently, composite theory has been the basis of a great number of researches to produce novel anti-microbial textiles.

Hydrophobic surfaces: Very low surface energy materials and nano-scale roughness structures (created by nanoparticles) are required for creating a super hydrophobic self-cleaning surface. Low surface energy substances make water roll off and easily wash off unattached dirt from surface. Different methods can be employed for creating nano-roughness. To make super hydrophobic surfaces, materials containing polymer nanoparticles were applied to the surfaces.

Wear resistant nanocomposites for engines: Scratch and wear are criteria parameters which will be considered for the metal parts used in automobile engines. Nanocomposites containing various reinforcements have been utilized to improve metal parts of engine against abrasion and wear. Reducing the scale of materials microstructure like grain size, particle size or layer thickness can significantly alter its properties.

Heat transfer improvement using nanocomposites: Nano particles added to the cooling agent showed significantly enhanced thermal conductivity of the liquids using these nano-metric materials. It has been found that reducing particles' size results in further increase in thermal conductivity of the liquid. Carbon nanotube is found effective nano-particle to enhance thermal conductivity.

1.3 FRACTURE MECHANICS

A material is said to fractured if maximum tensile stress or maximum extension in a body exceeds a certain threshold value. The strength of the material was basically considered to be dependent on the material properties. If effect of fracture on the strength was not taken into account or not understood properly then this sometimes resulted in a very high theoretical strength values, but practically the strength of the material was lower than the actual. One of earliest recorded incidents of brittle fracture failure was the Montrose bridges 1830 [21]. There have been many incidents due to fracture failure after that e.g the event of Tay Rail Bridge failure in 1879. All this led people to think about the fracture strength of the material. During the years of 1930 to 1950, fracture failure of commercial jet airplanes and welded ships further aggreviated the mechanicians. Up to that time Griffith's and Irwin's work has led the foundations for a new engineering branch "Engineering Fracture Mechanics" to flourish, and soon after that fracture mechanics evolved as an important engineering branch and a lot of research work was started, which made fracture mechanics [21].

1.3.1 Griffith's Work

The early strength theories were based on maximum tensile stress and in this connection tensile strength were used to find the material fracture strength. The fracture strength of the material is considered to be size independent. It was after Griffith's work that the concept of

size dependence on material strength was explicitly understood. The key points that motivated Griffith were

(i) The measured fracture stress of a bulk glass is around 100Mpa.

(ii) The theoretical fracture strength to break the atomic bond is much higher, 10GPA (approx, ten times higher).

Griffith himself performed experiments on glass fibers and observed that the fracture strength increases with a decrease in thickness of the fiber and vice versa. The observations were in agreement with the known fact, that strength of material is one-tenth the strength deduced from physical data. He attributed this behavior due to the presence of microscopic cracks/flaws in the bulk material.

To support his argument Griffith performed an experiment on a thin glass plate and introduced in it a large crack. He found that the breaking load of a thin plate of glass having in it sufficiently long crack normal to the applied stress, is inversely proportional to the square root of the flaw length .

$$\sigma = \sqrt{\frac{1}{a}} \tag{1.1}$$

or we can state that

$$\sigma\sqrt{a} = C \tag{1.2}$$

where a is the flaw length. The answer to such a behavior is not available in linear elasticity as it predicts the stress to be infinite in linear elastic material at the crack tip. Griffith used energetic approach to the problem. Creation of two new surfaces (crack) increases the surface energy of the body. Now the question whether a body will remain stable after crack growth, depends on the fact whether the body has sufficient energy to afford formation of new surfaces. In order to find constant C of equation 1.2, Griffith make use of energy balance of a body. He took a reference state of a glass fiber with no crack or flaw and loaded it with a uniform tension. He then calculated the potential energy stored in the body. Then he fixed the remote boundary so that the applied load does not do extra work and then he introduced a flaw of length a into the specimen. At the same time, creation of two new surfaces increases the surface energy,, of the body. The change of total free energy from reference state due to crack is thus Surface energy minus elastic strain energy that is the total or free energy.

1.3.2 Irwin's Work

The Griffith's work was largely ignored due to the fact that the Griffith's theory does not give good solutions for all materials and especially for metals, where the realistic energy required for the fracture was orders of magnitude than the surface energy. The studies conducted by Orawan and Irwin during 1948 [21] showed that even the fracture in brittle materials, there is extensive plastic deformation at the crack surface and hence a source of energy dissipation. The effect of plastic zone in brittle materials will be small as compare to the strain energy dissipated by the formation of the crack, but in case of ductile materials, it plays a vital role. As the load on the body is increased, the plastic zone develops behind the crack tip, the size of the plastic zone increases with the increase in load and at critical load the material starts unloading. Cycles of loading and unloading releases the energy in the form of heat. All these thoughts led to an important modification in the Griffith's work where a plastic work term is added into the energy balance equation to take into account the plastic work at the crack front [21].

CHAPTER 2

LITERATURE REVIEW

Langer *et al.* [1] investigated the material's macroscopic properties with the help of two public-domain programs that jointly predict behavior. To investigate the microstucture program OOF2 was used that start from an image of the microstructure and end with results from finite-element calculations. The mechanical properties were determined by OOF2 modelling and compared their results with the analytical models.

Vedula *et al.* [2] investigated the microstructure-level stresses occur in nanocomposite during processing. Depending on the grain size, the magnitude of these stresses can be sufficiently high to cause spontaneous microcracking when cooled from the processing temperature. They are also likely to affect where cracks initiate and propagate under loading. The magnitudes of stresses in samples was predicted using object-oriented finite-element analysis. Crack initiation and propagation was simulated, using a Griffith fracture criterion.

Cannillo *et al.* [3] investigated the fracture behavior of a composite material constituted by a glass matrix reinforced by means of a numerical model. The material was characterized by the presence of thermal stresses that arise upon cooling from the processing temperature due to the mismatch between the matrix and the reinforcements. The crack propagation was studied using finite elements coupled with selected failure criteria (Griffith) implemented inside the elements. Computational determination of crack propagation during failure was compared with obtained experimental data and microscopy images of crack interactions and the model provided results in good agreement with the experimental observations.

Cannillo *et al.* [4] studied the effect of pores on the fracture behavior of brittle solids. Object oriented finite element analysis was adopted, so that the effect of 2-D microstructural features on the mechanical response of the material can be determined. Firstly, microstructures of porous glass bodies containing isolated pores were considered. These specimens were numerically investigated in terms of fracture initiation and propagation: the numerical model

predicted that larger pores initiate fracture. The study confirms the suitability of the 2-D code to investigate the mechanical and fracture behavior of porous materials.

Liu *et al.* [5] analyzed the effect of clay fraction in epoxy/clay nanocomposites. Transmission electron microscopy showed the clay morphologies throughout the matrix a microscopic and homogeneous dispersion of clay. Mechanical analysis indicated a steady increase in modulus and a gradual decrease in high transition temperature as the clay loading increased. The fracture toughness of the nanocomposites was significantly increased with increasing clay concentration.

Wang [6] analyzed the microstructure of epoxy/clay nanocomposites. It was characterized by means of optical microscopy and transmission electron microscopy (TEM) and found that clay was uniformly dispersed in the resulting nanocomposite. Characterizations of mechanical and fracture behaviors revealed that Young's modulus increases with increasing the clay concentration while the fracture toughness shows a maximum at 2.5 wt % of clay. The micro deformation and fracture mechanisms were investigated by studying the microstructure of crack tips and the damage zone using TEM and scanning electron microscopy (SEM).

Cannillo *et al.* [7] investigated the effect of reinforcement on the overall composite mechanical behavior. The glass–matrix composite was fabricated by addition of molybdenum particles in various volume fractions. Investigated the effect of metallic particulate reinforcement, a FEM based numerical model was prepared. The study was focused on the fracture response of the composites. By the study of crack propagation patterns the effect of reinforcement volume fraction on composite fracture toughness was studied. Microscopy observations of fracture surfaces was performed to support the numerical results.

Bondioli *et al.* [8] carried out SEM analysis on the silica-epoxy nanocomposites. Mechanical properties were modeled by using a finite element code OOF2 which was able to construct a numerical model from a microstructural image of material. A more reliable model was prepared by considering the presence of an interphase layer surrounding the particles with intermediate elastic properties between the epoxy and the inclusions.

Wetzel *et al.* [9] analyzed the effect of reinforcement on mechanical and fracture properties of epoxy resins. Study was carried out on series of nanocomposites containing varying amounts of reinforcements. The mechanical performance of the nanocomposites was characterized, by fracture mechanics approaches (LEFM) and fatigue crack growth testing (FCP). The mi-

crostructure of specimens and the fractured surfaces were examined by TEM and SEM techniques in order to identify the relevant fracture mechanisms involved. It was found that the presence of nanoparticles in epoxy induces various fracture mechanisms, e.g. crack deflection, plastic deformation, and crack pinning. At the same time, nanoparticles can overcome the drawbacks of traditional toughening by simultaneously improving stiffness, strength and toughness of epoxy.

chawla *et al.* [10] performed object-oriented finite element modelling is used to evaluate the mechanical behavior of SiC particle-reinforced Al composites. Then compared the results of the Young's modulus and the stress-strain relations from the object-oriented model with the results of the experiment and the numerical results from simplified models. Their results indicate that 3D microstructure-based model can accurately predict the properties of particle-reinforced composites, while the simple analytical models can not as they do not account for the microstructural factors that influence the mechanical behavior of the material.

kaiyang *et al.* [11] analyzed the fracture behavior of the epoxy/aluminium oxide nanocomposites by TEM images. The mechanical properties of the nanocomposites was improved by adding nano-sized Aluminium oxide particles. It was found that platelet shape particles had better effects in terms of dispersion and improvement of the mechanical properties in comparison with the rod shape Aluminium oxide particles.

Cannillo *et al.* [12] studied the mechanical properties in glass–alumina composites. The numerical results proved that microstructural defects, such as pores, deeply influenced the fracture and other mechanical properties. On the contrary, the minimization of the mismatch in the coefficients of thermal expansion of the reinforcement materials allowed to obtain low thermal residual stresses. In order to support the numerical model, the experimentally observed crack paths were compared to the computationally predicted ones.

Dong *et al.* [13] analyzed the numerical approach, object-oriented finite element (OOF) technique to incorporate the SEM into two-dimensional finite element modelling. SEM were utilised to generate the geometric micro/nano structure. Numerical results predicted the tensile properties of polypropylene (PP)/organoclay nanocomposites. Their results indicated that Their results indicate that 2D microstructure-based numerical model can accurately predict the properties of nanocomposites.

Hu *et al.* [14] studied three different approaches of micro-nanomechanics. and numerical

analysis on predicting mechanical properties of nanocomposites. Three different approaches were discussed in finite element modeling, i.e. multiscale representative volume element (RVE) modeling, unit cell modeling, and object-oriented modeling. They concluded that object-oriented modeling captures the exact shape and morphology of the nanocomposites and able to capture all the feature taking morphological image as input.

Wang *et al.* [15] carried out computational study in effect of structures of nanocomposites on their elastic properties. They developed special program code for the automatic generation of 3D multiparticle unit cells for nanocomposite modelling. The effects of the effective interface properties, particle sizes, particle shapes and volume fraction of nano reinforcement on the mechanical properties of nanocomposites are studied in numerical experiments and analyzed that higher degree of particle clustering leads to lower Young's modulus of the nanocomposites.

Dai *et al.* [16] studied the initiation and growth of microcracks in the nanoclay reinforced composite was analyzed in numerical experiments using 3D micromechanical unit cell models. For automatic generation of FE unit cells an original program code was developed. For analysis different crack growth criteria were compared. It was observed that the increasing aspect ratio leads to the increasing Young modulus, but decreasing strength and the clustering of disks had an adverse effect, meaning increased strength and lower stiffness.

sharma *et al* [17] studied the mechanical and thermal properties of phase composites (IPCs) of Ni-Al2O3 using finite element based object-oriented program (OOFEM). In order to understand the material behavior, OOFEM combines the images with the fundamental material properties. Thermal conductivity, thermal expansion coefficient, and modulus of elasticity for the composites were examined using OOFEM and compared with other analytical methods which show good agreement with the numerical modelling.

CHAPTER 3

PROBLEM DEFINITION AND OOFEM MODELLING

3.1 PROBLEM DEFINITION

To model nanocomposites there are different techniques such as multiscale RVE modelling, multiscale unit cell modelling and object-oriented modeling. In both multiscale RVE modelling and unit cell modeling, two basic assumptions are made. First, nanofillers can be idealized to simple geometries for instance spheres, ellipsoids, cylinders, or cubes and second, nanocomposites can be reproduced by assembling a large number of such RVEs or unit cells. These assumptions lead to serious limitations in analysis of nanocomposites. An object-oriented finite element code, OOF is developed by National Institute of Standards and Technology (NIST). It requires the microstructure of nanocomposite with the material properties for conducting finite element analysis. To develop real mapping of nano/microstructures it takes the SEM (scanning electron microscopic) images as an input which provides all the information about the microstructure. The computer program generates the orphan meshes and capable of mapping all the features of complex geometry.

3.2 MODELLING OF EPOXY-CLAY NANOCOMPOSITE

There are different material modelling methods to predict the microstructural properties of the material as shown in figure 3.1. Using FEM an attempt is made to study the mechanical property of the epoxy-clay nanocomposite. This technique is used for various composites/heterogeneous materials using the software OOF2 [22, 23].

This open source finite element method software is developed by NIST and available at NIST, USA website. It is an effective software for image based material analysis because of its some special features

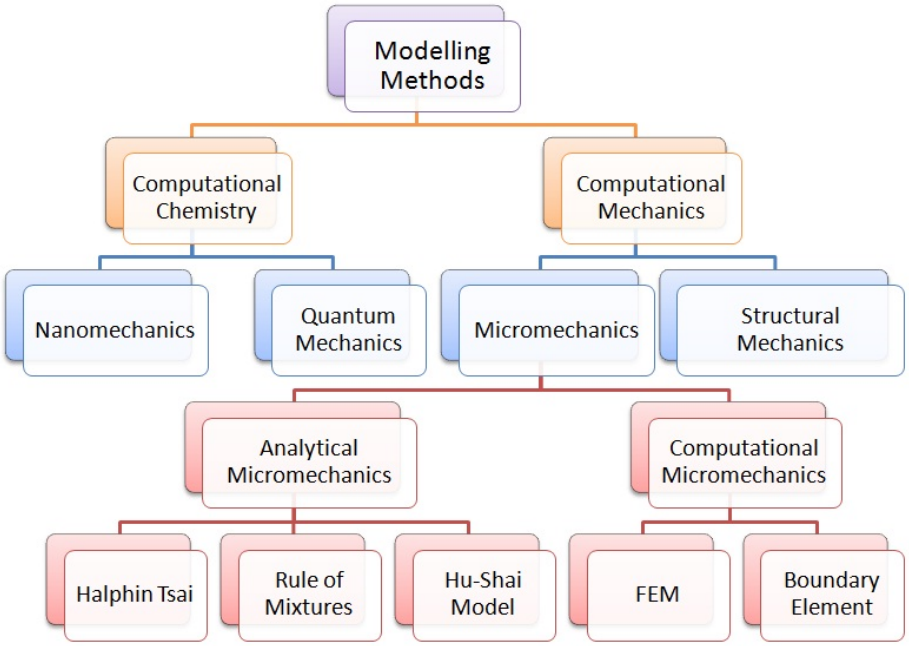

Figure 3.1: Material modeling techniques [24]

The modelling of microstructure involves various steps. It starts with taking SEM as input and defining finite element model by doing pixel selection, skeleton formation, mesh generation, equation formulation and boundary conditions as shown in fig.3.2.

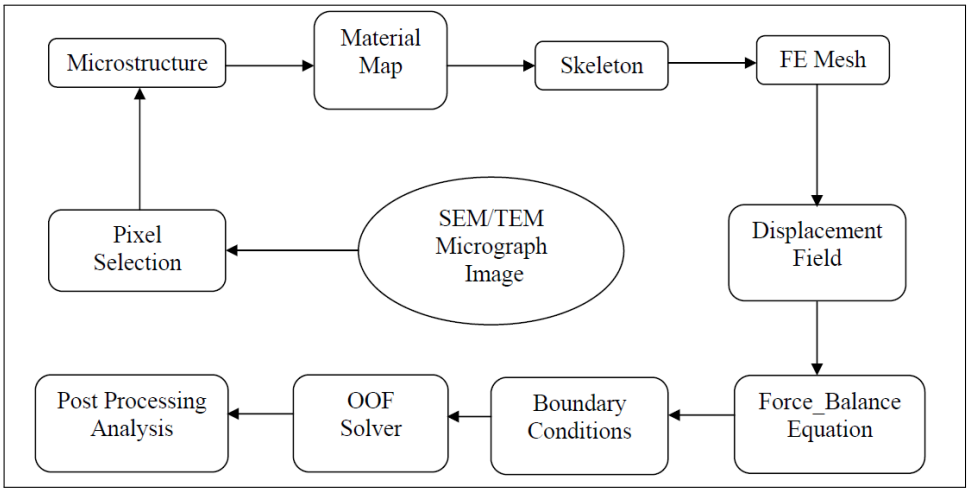

Figure 3.2: Steps for OOF modelling [13]

3.2.1 Inputs required for OOF2 modelling

The program OOF2 is based on the SEM images, which collect all the microstructural features of the nanocomposite. There are many tools for image improvement like detection of edges, boundary filters etc. There is no fixed rule which predicts which tool should be applied on

certain stage, it only depends on the nature of the image to be processed.

3.2.2 Image processing

The image imported in OOF2 is simply a microstructure and it does not contain any useful information. To make it more meaningful image segmentation is done. Different constituents of the heterogeneous material are identified by selecting pixels from the image and assign a pixel group in the image. Image segmentation means to separate different materials from the microstructure.The different options for pixel selection are by point, pixel selection by circle, burn and color.

The modelling of microstructure is done on an effective portion of the SEM. The portion which carry all important features of the microsctructure is termed as an effective portion. The grey portion in the SEM is nanoclay and the black portion represents the epoxy material. The captured image clearly shows the different components of heterogeneous material.

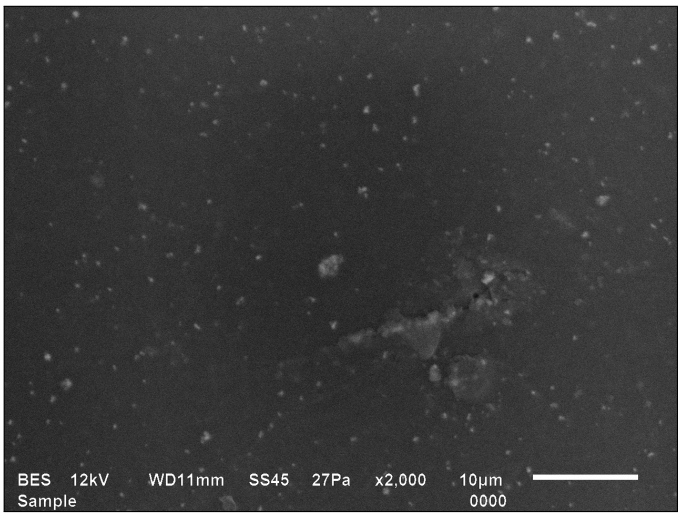

Figure 3.3: captured SEM image portion

3.2.3 Volume fraction measurements

To determine Young's modulus analytically, the value of filler volume fraction is needed. Volume fraction was calculated as

$$\phi_f = \frac{V_f}{V_m + V_f} \tag{3.1}$$

where V_f, V_m are the values of volume percentage of filler, matrix respectively. In case of epoxy-clay nanocomposite volume fraction is to be calculated from the SEM. Volume percentage of filler from SEM is calculated by the method described in the optical microscopy primer [37].

The metric properties of a structure such as the volume fraction, surface area, length, and curvature, can all be determined by stereological rules. To method to measure the volume fraction, in this case epoxy-clay nanocomposite is described below.

Assuming that the images are representative of the specimen, the total area of the clay can be determined by counting pixels and the volume fraction is measured by the area fraction. However, a preferred method for estimating the volume fraction is carried out by placing a

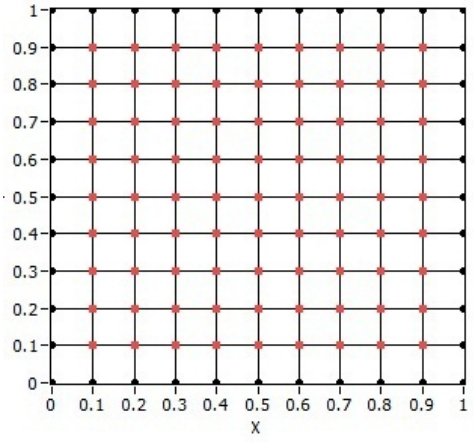

Figure 3.4: Sparse grid of points [33]

sparse grid of points on the image, example is shown in figure.3.10

Counting the fraction of those points that "hit" or fall on the structures of interest. This might seem like a less accurate measurement, but it has several advantages. The statistics of counting independent events provides a direct estimate of the measurement precision. In SEM the estimates of volume fraction for each field of view obtained by the area measurement and the grid point count are not too dissimilar, while the variation from field to field is considerable. The effective portion of the SEM is divided into four parts. In first image and the point grid view is shown in figure.3.5

in first case only two points lie on the selected pixels so the point fraction in this case is 2/25 which is equal to 8%. Similarly in second, third and forth SEM the point fractions are 2/25, 2/25, 3/25 respectively which are equals to 8%, 8%, 12%. The average volume fraction is shown in the table 3.1

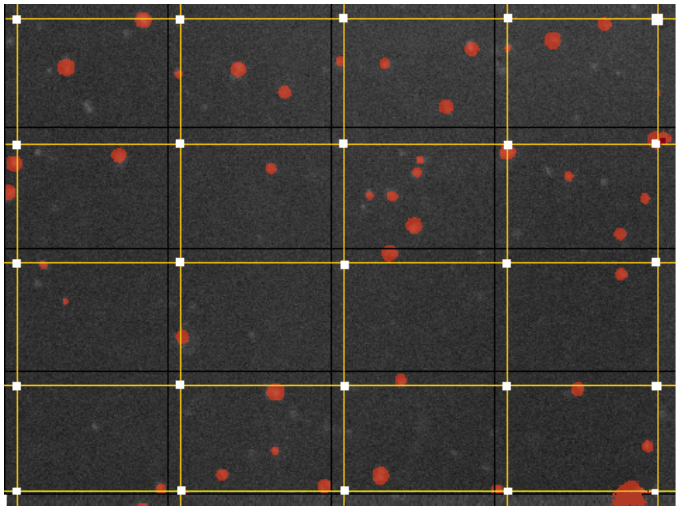

Figure 3.5: Sparse grid of points on first image

Table 3.1: Average volume fractions of epoxy-clay Nanocomposite.

Region	**Point fraction**
First	8%
Second	8%
Third	8%
Forth	12%
Average	9%

It is important to examine enough fields of view to obtain a representative sample of the specimen, and the point count method generally insures this. The area is measured by counting pixels, this is not the same as the use of the grid because the pixels are close together. For the square root of the number of hits to be a valid estimate of the precision of the count, the points must be independent samples of the structure, meaning that the grid must be sparse enough that the points rarely fall on the same feature.

3.2.4 Image segmentation

Image segmentation means picking up different pixels of same material from SEM. This process is done by various options in the pixel selection tool box. The example shown in figure 3.6 represents the process of pixel selection. The image segmentation of epoxy clay

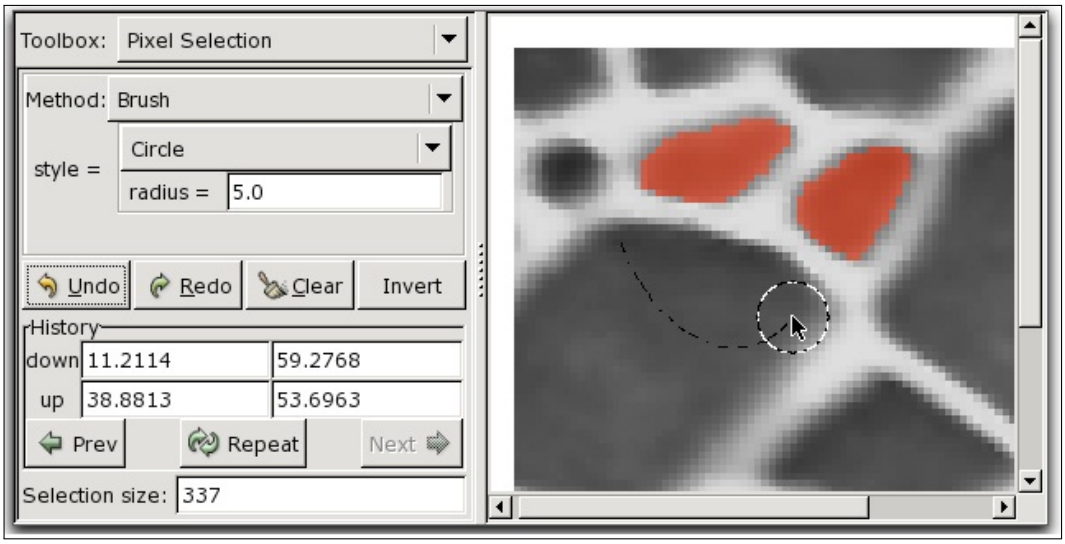

Figure 3.6: image segmentation using pixel selection [37]

nanocomposite is shown in figure 3.7. The selected pixels of different constituents forms the

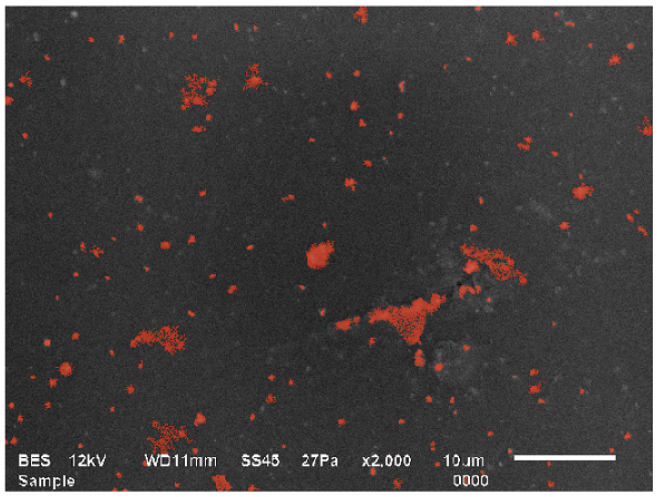

Figure 3.7: image segmentation using pixel selection

pixel group. The material properties are assigned to these pixel groups. This mapping of material constituents makes the finite element model more accurate.

3.2.5 Assigning material properties

The materials in OOF2 exist independently of microstructures. The Materials Page consists of two panes, as shown in Figure 3.8. The property pane is for setting the parameters for properties. The Material pane creates and manipulates materials and assigns them to pixels in a microstructure.

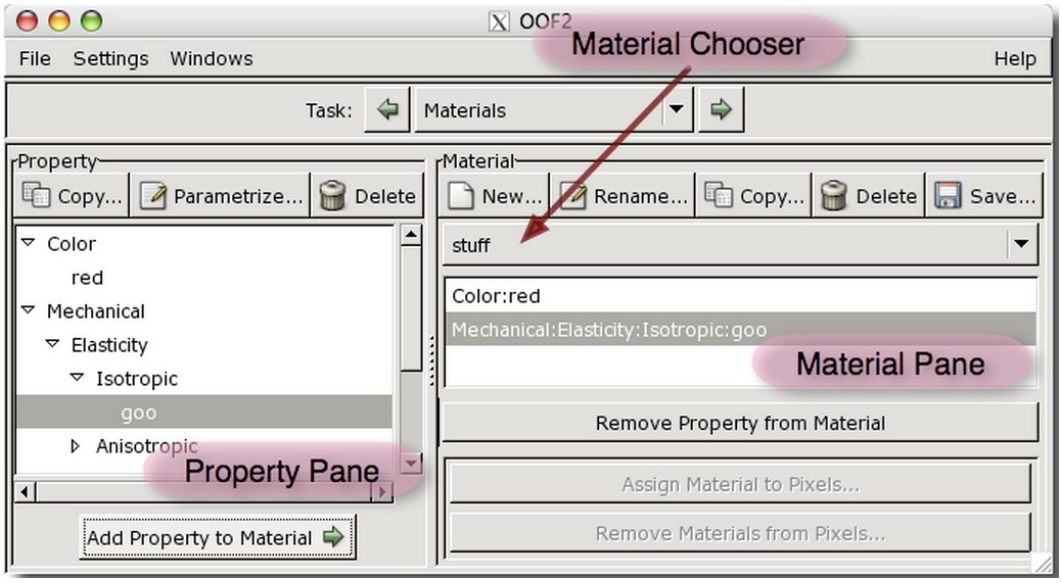

Figure 3.8: Material page [37]

Property pane contains hierarchical list of material properties. The table 3.2 shows the mechanical properties assigned to the epoxy/clay nanocomposite.

Table 3.2: Material Properties of Epoxy-clay Nanocomposite [34]

Material properties	**Epoxy**	**Clay**
Young's modulus(GPa)	3.034	4.6
Poisson's ratio	0.40	0.26
Thermal conductivity ($W/m-^oK$)	1.4	0.8
Thermal expansion coefficient ($\mu m/m^oC$)	62	35.1

.

The properties shown in the table 3.1 are assigned to the groups identified as either epoxy or nanoclay. The interface properties are not considered in the OOF2. The interface properties are different from matrix and reinforcement.

3.2.6 Skeletons

The next step in OOF is to create skeleton before creating a finite element mesh. The skeleton defines only the geometry of the mesh. It does not include any information about equations, fields or finite element shape functions. All of that information is in the mesh class, which will be discussed later. The skeleton is an intermediate step between the pixelized microstructure and the finite element solution. It represents the finite element discretization of the microstructure. One microstructure may contain many skeletons, representing different discretizations. One skeleton, in turn, may generate many meshes, allowing different physics or different solution methods to be tried in a single geometry. The skeleton task page contains tools for creating and modifying skeletons. The skeleton info toolbox contains tools for examining the details of a skeleton in the graphics window. Skeleton elements inherit their material property from the pixels beneath them in the microstructure. If the skeleton geometry is to be a good approximation of the microstructure geometry, then all of the pixels lying beneath an element should have the same assigned material. The homogeneity of a skeleton element is a measure of how well the element achieves this goal. The homogeneity is computed by finding the area of the element that overlies each category of pixel. Pixels that have different assigned material or belong to different meshable pixelgroups are in different categories. The category claiming the largest area of the element is the dominant category [37]. The homogeneity is defined as the ratio of the area of the dominant category to the area of the element as a whole. A completely homogeneous element has a homogeneity of 1.0.

An element made up of N equal components has a homogeneity of 1/N. The material assigned to an element is the material of its dominant pixel category. The first step in skeleton generation is formation of the rectangular or square grid of elements then by different tools present in the skeleton task page it is modified. The development stages of the skeleton are shown in Fig 3.9

Many of the tools for modifying skeleton such as anneal and smooth work by reducing an effective energy functional, E, of the mesh. This functional assigns a number between 0 and 1 to each element. It is called an energy because of its role in the annealing operation, where it plays the role of the energy in a statistical mechanical simulated annealing process. The energy functional has two contributions, a homogeneity, E_{hom} and a shape energy, E_{shape}. Their relative importance is controlled by a parameter $\alpha = 0$

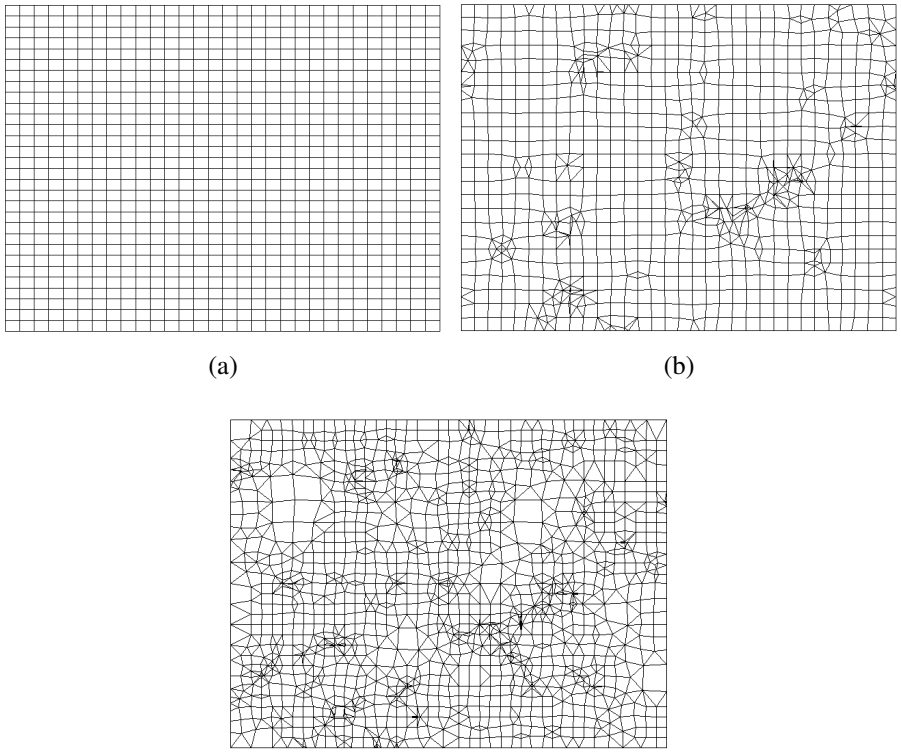

Figure 3.9: Skeleton development stages (a) Quad skeleton initiation of epoxy-clay nanocomposite, (b) skeleton moving stages, (c) developing skeleton

$$E = \alpha E_{hom} + (1 - \alpha) E_{shape} \tag{3.2}$$

When $\alpha = 1$ then Skeleton modifications that use E will not consider the shape of elements at all, and will result in homogeneous but badly shaped elements. When $\alpha = 0$, modifications will not consider homogeneity, and will result in well shaped but possibly inhomogeneous elements. When $0 < \alpha < 1$, there will be a trade-off between shape and homogeneity as shown in Fig 3.10.

3.2.7 Meshing

The OOF2 Mesh object represents an actual finite element Mesh. It combines the geometry of a skeleton with information about equations and boundary conditions, and it stores the values of displacements.

Every mesh is derived from a skeleton. The mesh elements have the same shape and position as the associated skeleton elements. The material assigned to each mesh element is

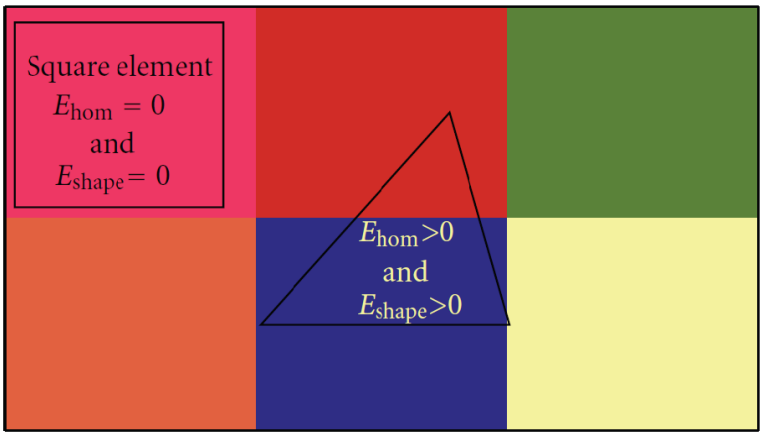

Figure 3.10: Energy Factor [37]

the material of the dominant pixel category of its skeleton element. A single skeleton may give rise to more than one mesh [37].

The polynomial order of the element shape functions determines the order of the interpolation within the element, and therefore affects the accuracy of the solution for e.g; (Fields computed with linear shape functions will be constrained to have constant gradients within elements) Because shape functions values are 1 at present node and 0 at all others, the number of nodes along an element edge determines the order of the shape functions: an edge with nodes only at its endpoints must have linear shape functions, whereas an edge with nodes at its endpoints and one more in its interior must have quadratic shape functions. The completed formation of mesh is shown in Figure 3.11.

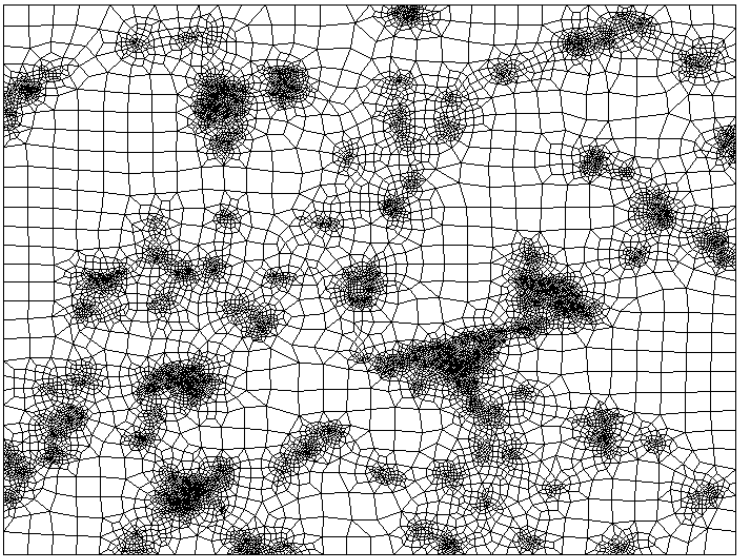

Figure 3.11: Formation of mesh

There are actually three kinds of nodes: nodes used to store field values (function nodes),

nodes used to determine the element geometry (mapping nodes), and nodes used for both purposes. Nodes determine element geometry by defining a mapping from a "master" element with a standard shape and position to the actual element.

The mapping nodes of the master element are mapped to the nodes of the actual element, and all other points are mapped by using the mapping nodes' shape functions for interpolation. Non-linear mapping can produce elements with curved edges. Elements with the same number of function and mapping nodes are called isoparametric. Elements with more function nodes than mapping nodes are called subparametric, and elements with more mapping nodes than function nodes are called superparametric.

3.2.8 Fields and Boundary Conditions

After creating a mesh, the next step is to give boundary conditions. OOF2 can solve problems for displacement, temperature, and voltage fields. The characteristics which are computed as secondary characteristics are not considered as field in OOF2. For example, heat flux is a field in the sense that it has values everywhere in the continuum, but in OOF2, it is computed as secondary characteristic and not as a fundamental quantity hence it is not considered as a field in OOF2 software. Divergence equations and plane-flux equations are the two types of equations that OOF2 can solve. OOF2 supports five kinds of boundary conditions: Dirichlet, Neumann, floating, generalized force, and periodic [37]. The boundary conditions implemented are given in table 3.3.

Table 3.3: Boundary conditions

Dirichlet condition	$u_x = 10$ at right side $u_y = 0$ at bottom side $u_y = 0$ at left side
Equation	Force balance
Field	Displacement

Dirichlet boundary conditions assign fixed values to Fields. A separate boundary condition must be established for each component of a Field that is to be fixed. Dirichlet boundary conditions may be applied to both Edge and Point boundaries.

3.3 COMPOSITES THEREOTICAL MODELS

3.3.1 Halpin-Tsai Model

There are some theoretical mathematical models which are use to calculate the mechanical properties of the the composites. These models can also be applied to the nanocomposite. There are some assumption which make the models less accurate but the most extensively used model is Halpin-Tsai model, to determine the tensile modulus of nanocomposites. It determines the elastic modulus as the function of portion ratio. The elastic modulus of composite in Halpin-Tsai model is intended as

$$\frac{E_C}{E_m} = \frac{1 + \zeta\eta\phi_f}{1 - \eta\phi_f} \tag{3.3}$$

This model can be applied to almost every type of reinforcement geometry for instance flake or fiber like reinforcements. The term's E_c, E_f, E_m are the values of elastic modulus of compound material, reinforcement and the matrix. ϕ_f is the reinforcement volume fraction ζ is the shape factor depend upon the morphology of the reinforcement geometry. Its value is 2(l/t) is used for the disk like particles where l, d, t are the length, diameter and thickness of the reinforced particles in the matrix. Two dimensional reinforcement particles of clay have less impact than the one dimensional fiber like reinforcement. To neglect this effect in Halpin-Tsai model a elastic modulus reduction factor (MRF) whose value is 0.66 [27] is introduced.

$$\frac{E}{E_m} = \frac{1 + \zeta(MRF)\eta\phi_f}{1 - \eta\phi_f} \tag{3.4}$$

3.3.2 Hui-Shia Model

This model is similar to previous model and it calculates the elastic modulus of composite. In this model the approximation used is that there is faultless interfacial bonding between the

matrix and the reinforcement. The Hui-Shai model is expressed as

$$\frac{E_c}{E_m} = \frac{1}{1 - \frac{\phi_f}{4}[\frac{1}{\xi} + \frac{3}{\xi + A}]} \tag{3.5}$$

The Term E_c, E_f, E_m are the values of elastic modulus of compound material, reinforcement and the matrix.

$$\xi = \phi_f + \frac{E_m}{E_f - E_m} + 3(1 - \phi_f)[\frac{(1-g)\alpha^2 - \frac{g}{2}}{\alpha^2 - 1}] \tag{3.6}$$

$$\Lambda = (1 - \phi_f)[\frac{3(\alpha^2 + 0.25)g - 2\alpha^2}{\alpha^2 - 1}] \tag{3.7}$$

$$g = \frac{\pi}{2}\alpha \tag{3.8}$$

where alpha is inverse aspect ratio of the reinforcement and α is ratio of thickness to length for disk-like particles.

3.3.3 Voigt Upper Bound and Reuss Lower Bound

A general rule of mixtures is a weighted mean used to predict various properties of a composite material. It provides a theoretical upper- and lower-bound on properties such as the elastic modulus, mass density, ultimate tensile strength, thermal conductivity, and electrical conductivity. It is possible to model or estimate the effective elastic modulus of nanocomposie in terms of the properties of the various constituent materials. To do it precisely one must incorporate the individual elastic modulus of the constituents, the volume fractions of the constituents, geometric details of how the various constituents are arranged. The geometric details are the most difficult to know or measure. If the details of geometry are not known then the best is to estimate upper and lower bounds on the modulus. The Hui-Shia Model becomes the Voigt rule of mixtures (ROM) when the value of zeta reaches to the infinity. This uses one assumption of isostrain, conditions that strains in matrix and reinforcement are same. In general, for material property E (elastic modulus), the rule of mixtures states that the overall property.

The upper bound limit is as follows

$$E_c = \phi_f E_f + (1 - \phi_f) E_m \tag{3.9}$$

The Hui-Shia Model become the lower bound.This uses the assumption of isostress approach that there is uniform stress between the matrix and the reinforcement. This is also called as Reuss inverse rule of mixtures (IROM). The bounds are powerful and robust tools. They give rigorous upper and lower limits on the modulus, given the composition. If measurements fall outside the bounds, then there is some mistake in volume fractions, or composition.

The lower bound limit is as follows

$$\frac{1}{E_c} = \frac{\phi_f}{E_f} + \frac{(1 - \phi_f)}{E_m} \tag{3.10}$$

In upper and lower bound the elastic modulus is calculated by taking volume fraction as input irrespective of filler shape/geometry, orientation and spatial arrangement. Similarly the ROM and IROM are used to calculate the thermal conductivity of composite materials. The ROM and IROM for thermal conductivity is as follows

$$(\frac{f}{k_f} + \frac{1 - f}{k_m})^{-1} \leq k_c \leq f k_F + (1 - f) k_m \tag{3.11}$$

3.3.4 Turner Model

There are some theoretical mathematical models which are use to calculate the thermal properties of the the composites. The most extensively used model is Turner model [31], to determine the thermal conductivity of nanocomposites. The thermal conductivity of composite in Turner model is intended as

$$\alpha_C = \frac{\alpha_m K_m V_m + \alpha_p V_p K_p}{K_m V_m + K_p V_p} \tag{3.12}$$

where α is the linear coefficient of thermal expansion, volume fraction is V, bulk modulus is K, and the subscripts c, m,and p denote the composite, matrix, and reinforcement,respectively.

3.3.5 Schapery Model

Another model to calculate thermal conductivity of Epoxy-clay nanocomposites is Schapery Model [32]. The upper and lower bounds of the linear thermal expansion coefficient were given by Schapery as follows

$$\alpha_c = \alpha_m V_m + \alpha_p V_p + [\frac{4G_m}{K_c}][\frac{(K_c - K_p)(\alpha_m - \alpha_p)V_p}{4G_m + 3K_p}] \tag{3.13}$$

The lower bound given by Schapery is same as upper bound, with interchange of subscripts p and m as follows

$$\alpha_c = \alpha_m V_m + \alpha_p V_p + [\frac{4G_p}{K_c}][\frac{(K_c - K_m)(\alpha_p - \alpha_m)V_m}{4G_p + 3K_m}] \tag{3.14}$$

Where K_c is the bulk modulus of the composite as evaluated in case of Hashin and Shtrikman bounds. Here we consider K_c as the average of the upper and lower bounds, K_{upper} and K_{lower} of the bulk modulus, for our analysis. The value of upper and lower bounds,K_{upper} and K_{lower} is as follows:-

$$K_{upper} = K_p + (1 - V_p)[\frac{1}{(K_M - K_p)} + \frac{3V_p}{(3K_p + 4G_p)}]^{-1} \tag{3.15}$$

$$K_{lower} = K_m + V_p[\frac{1}{(K_p - K_m)} + \frac{3V_p}{(3K_m + 4G_m)}]^{-1} \tag{3.16}$$

3.4 FRACTURE MECHANICS

In the FE package there are privileges to model crack initiation and crack propagation. The XFEM is a numerical method, based on the Finite Element Method (FEM),that is especially designed for treating discontinuities. Discontinuities are generally divided in strong and weak discontinuities. Strong discontinuities are discontinuities in the solution variable of a problem.

In structures, the solution variable is usually the displacements so strong discontinuities are displacement jumps, such as cracks and holes. Weak discontinuities are discontinuities in the derivatives of the solution variable. In structures such discontinuities would involve kinks in the displacements (jump in the strains), as for example in bi-material problems. In this case

all simulations are done in Abaqus(XFEM) for the 2D cracked domain case [21].

XFEM is available for three-dimensional solid and two-dimensional planar models, three-dimensional shell models are not supported. In abaqus the analysis on the onset and propagation of cracking problems using the extended finite element method (XFEM) can be performed. The XFEM can be applied to parts containing geometry, orphan meshes, or a combination of both.

In nanocomposite case there is no geometry because the meshes are generated by image processing technique (OOF2) so the orphan meshes. In the analysis, the initial location of the crack is defined the propagation is predicted by the XFEM. Abaqus, determines the location of the crack during the analysis based on the value of the maximum principal stress or strain calculated in the crack domain.

The Abaqus(XFEM) have several limitation:-

(i) only the STATIC analysis procedure is allowed.

(ii) only linear continuum elements are allowed (CPE4, CPS4, C3D4, C3D8) with or without reduced integration.

(iii) no parallel processing of elements.

(iv) no fatigue crack growth.

(v) only one crack may exist within a particular element.

(vi) a crack may not turn more than 90 degrees within a particular element.

(vii) only one crack may exist within a particular element.

(viii) not available in Abaqus/Explicit.

3.4.1 Modelling of Crack and boundary conditions

Modelling of crack in Abaqus is done in the interaction module.The modelling space is 2D planar and its type is deformable.The base feature of the crack is wire and its size is 5.

In interaction module under the menu special there is option named crack and at that we can create two types of crack one is XFEM and other is seam. The location of the crack is shown in the Figure 3.12.

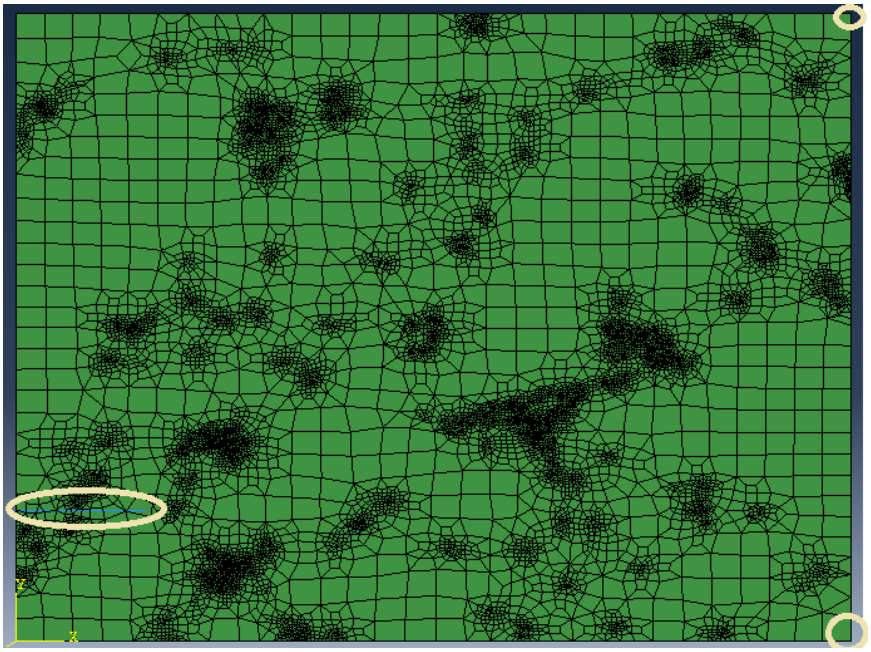

Figure 3.12: Crack Location

The boundary at bottom right corner of the domain U1, U2 and UR3 is zero. Its type is mechanical and step is displacement rotation. The boundary condition at the top right corner of the domain is zero at U1 and UR3 as given in table 3.4.

Table 3.4: Boundary conditions

Boundary condition	Pressure = 2 KN	at bottom and top edge
	U1 = UR3 = 0	at top right corner
	U1 = UR3 = UR2 = 0	at bottom right corner

Expand Field Output Requests,Expand the Failure/Fracture options and check to PHILSM, Level set value phi. This will allow viewing level set function defining the crack. The pressure at top and bottom of the nanocomposite 2 kN is applied.

CHAPTER 4

RESULTS AND DISCUSSIONS

4.1 MECHANICAL BEHAVIOUR OF EPOXY-CLAY NANOCOMPOSITE

The morphology and the structure of the epoxy-clay nanocomposite is analyzed in the object oriented program. The material properties of epoxy matrix and clay particles are given in the table 3.1. Young's modulus of epoxy nanoclay is first calculated in OOF2 then compared with results obtained from rule-of-mixtures approach, Hashin-Shtrikman analytical bounds [25], Halpin–Tsai [28] model. The Young's modulus value is 3 GPa calculated by using OOF2.

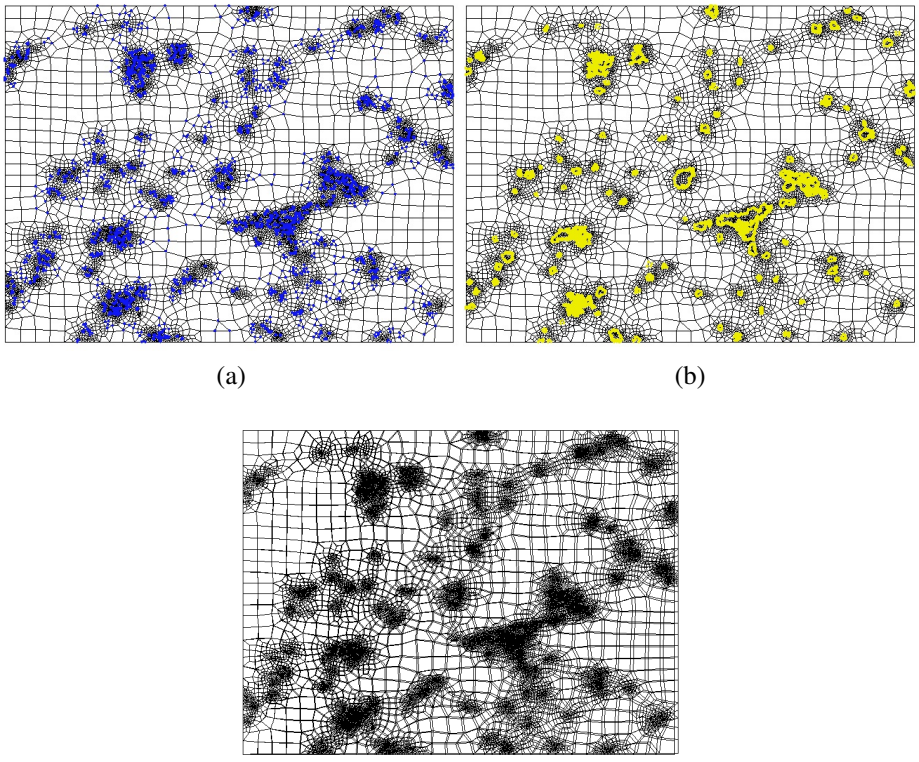

(a) (b)

(c)

Figure 4.1: Mesh deforming stages (a) nanoclay reinforcement, (b) nanoclay Boundaries, (c) deformed Skeleton

4.1.1 Validation of OOF modelling with rule of mixture approach

The Young's modulus obtained from the the OOF2 is compared with Voigt upper bound (rule of mixture) and with Reuss lower bound (inverse rule of mixture). The difference between the modulus is shown in the table 4.1. The calculated values of Young's modulus was lower

Table 4.1: Validation of OOF result with rule of mixture approach

Method	Young's Modulus
OOF2	3.0 GPa
ROM	3.174 GPa
IROM	3.129 GPa

than lower bound and upper bound. The value of upper bound is higher than value of OOF2 because ROM consider isostrain condition between the matrix and the reinforcement but in actual practice there is always non uniform strain between them. The other reason of its higher value is ROM do not take shape factor into consideration. It calculates value of modulus based on the filler volume fraction. OOF2 captures the exact shape and size of the reinforcement and do not consider isostrain condition between matrix and the reinforcement. This result in lowering the value of modulus.

4.1.2 Validation of OOF result with Halpin–tsai model

The Young's modulus obtained from the the OOF2 is compared with Halpin–Tsai Model. The difference between the modulus is shown in the Table 4.2. It can be observed that calculated

Table 4.2: Validation of OOF modelling with Halpin–Tsai model

Method	Young's Modulus
OOF2	3.0 GPa
Halpin–Tsai model aspect ratio 10	3.17 GPa
Halpin–Tsai model aspect ratio 100	3.18 GPa

value of Young's modulus show better agreement with the analytical model. The reason of mismatch between the two values may be due the properties of the interphase which are different from the matrix and filler also exist between them [29, 30]. These interphase properties are not measured in the OOF modeling. These properties may affect the complete mechanical behavior of the nanocomposite as a result of high specific surface area of clay particles. In Halpin–Tsai model curve with L/t = 10 shows better agreement with the numerical model.

4.1.3 Validation of OOF modelling with Hui-shia model

The modulus Young's obtained from the the OOF2 is compared with Halpin–Tsai Model. The difference between the modulus is shown in the Table 4.3. The calculated value of Hui-Shia

Table 4.3: Validation of OOF modelling with Hui-Shia model

Method	Young's Modulus
OOF2	3.0 GPa
Hui-Shia model inverse aspect ratio 0.1	3.16 GPa
Hui-Shia model inverse aspect ratio 0.01	3.18 GPa

model is higher. The comparisons of young's modulus with Hui–Shia model model two fixed inverse aspect ratios (t/l = 0.01 and t/l = 0.01) are considered. From the results it is observed that when In Hui-Shia model curve with t/l=0.1 shows better agreement with the numerical model.

4.2 THERMAL BEHAVIOUR OF EPOXY-CLAY NANOCOMPOSITE

The thermal behaviour of the epoxy-clay nanocomposite is analyzed in the object oriented program. The material properties of epoxy matrix and clay particles are given in the table 3.1. In the analysis boundary conditions at temperature 50^oC are used and comparing the same with the analytical models. While working with OOF2, the fixed temperature boundary conditions are applied so that the average temperature is 50^oC and steady state heat transfer condition can be assumed. The main objective of the analysis is to study the coefficient of

linear expansion and thermal conductivity of epoxy-clay nanocomposite. It is first calculated in the OOF2 then compared with Turner model [**?**], Schapery analytical bounds [32]model and ROM approach.

4.2.1 Comparison of thermal conductivity by OOF2 and ROM approaches

The Thermal conductivity obtained from the the OOF2 is compared with Voigt upper bound (rule of mixture) and with Reuss lower bound (inverse rule of mixture). The difference between the modulus is shown in the table 4.4. The thermal conductivity by using OOF2 is

Table 4.4: Thermal conductivity by OOF2 and rule of mixtures approach

Method	Thermal conductivity $(W/m -^o K)$
OOF2	0.95
ROM	1.346
IROM	1.04

slightly lower than ROM approach. This may be due to the assumption that there is isostrain between the matrix and reinforcement. There is a zero thermal contact resistance between the two constituents.

4.2.2 Comparison of thermal conductivity by OOF2 and Turner model

The Coefficient of Linear Expansion obtained from the OOF2 is compared with by Turner Model .The difference between the two is shown in the table 4.5.

Table 4.5: Thermal expansion coefficient by turner and OOF2 Model

Method	Thermal expansion coefficient $(\mu m/m^oC)$
OOF2	59
Turner model	60.4

4.2.3 Comparison of linear expansion by OOF2 and Schapery model

The Coefficient of Linear Expansion obtained from the OOF2 is compared with by schapery Model .The difference between the two is shown in the graph:- The values of coefficient lower

Table 4.6: Thermal expansion coefficient by OOF2 and Schapery model

Method	Thermal expansion coefficient ($\mu m/m^oC$)
OOF2	59
Schapery upper bound	60
Schapery lower bound	59.7

than the upper and lower bound of schapery model. As mentioned earlier the value of upper bound is slightly higher that is due to the fact that analytical model assumes isostrain conditions there is no thermal resistance present in the composite but in actual pratical applications there are always some thermal resistance between the different phases of the nanocomposite. Another reason may be the interphase properties are not measured in the OOF modeling. These properties may affect the complete thermal behavior of the nanocomposite as a result of high specific surface area of clay particles.

4.3 FRACTURE BEHAVIOUR OF EPOXY-CLAY NANOCOMPOSITE

The XFEM was used to evaluate the stresses and displacement at the crack tip where as OOF2 was used to capture the exact morphology and shape of the nanocomposites. For capturing the exact morphology and shape of the nanocomposite, OOF2 introduced triangular elements. However these traingular elements were considered bad shape elements in XFEM analysis. The complete analysis and deformed mesh is shown in Fig 4.2. Assumption in analysis

(i) Single edge crack was assumed for analysis

(ii) The location for the crack was assumed

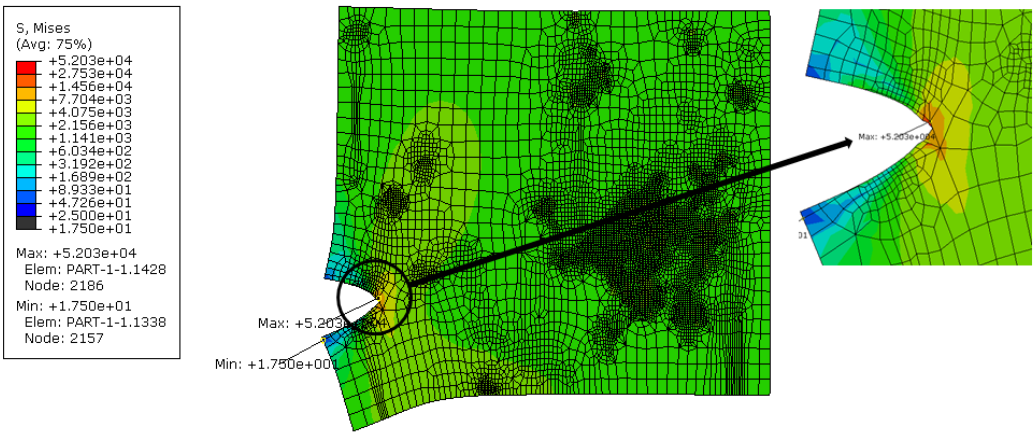

Figure 4.2: Crack Location

(iii) Initial length of the crack was assumed

Traingular elements in XFEM resulted in inaccurate analysis hence number of attempts were made to calculate the exact value of stress at crack tip.From the analysis, the average value of stresses at the crack tip was $5.2 * 10^4$N.

CHAPTER 5

CONCLUSION AND SCOPE FOR FURTHER STUDY

5.1 CONCLUSION

An attempt has been made to study epoxy-clay nanocomposites using the finite element analysis in order to study their mechanical and thermal properties. A comparison of mechanical properties estimated from different analytical models and OOF2 shows that OOF2 is an effective tool for evaluating material behavior under thermal and/or mechanical conditions, because it incorporates the actual microstructure of the material (including distribution, shape and size of particles). OOF2 prediction for 9 vol% clay-reinforced composites is lying between the upper and lower bond of Hashin-Shtrikman values. Young's modulus predicted using OOF2 differs from that of rule-of-mixture's predictions and within the range of 5%, where OOF2 predicts 4.4% lower value than that estimated using ROM methods. OOF2 results are more efficient and reliable results than that of rule of mixture which merely predicts on the basis of respective volume fractions and individual properties of constituents.

5.2 SCOPE FOR FURTHER STUDY

The present study carried out in dissertation may be further extended in the following directions:-

(i) The present study may also be carried out for other materials as well.

(ii) The problem may also be solved with other numerical method like boundary element method.

(iii) The different type of analysis can be performed by using same numerical method.

(iv) This type of analysis compared with different scales using multi modelling method.

(v) The present study may also be carried out for different fractions of reinforcements.

REFERENCES

[1] S. A. Langer, E. R. Fuller Jr, and W. C. Carter, "An image-based finite-element analysis of material microstructures," *Computing in Science & Engineering*, vol. 3, no. 3, pp. 15–23, 2001.

[2] V. R. Vedula, S. J. Glass, D. M. Saylor, G. S. Rohrer, W. C. Carter, S. A. Langer, and E. R. Fuller, "Residual-stress predictions in polycrystalline alumina," *Journal of the American Ceramic Society*, vol. 84, no. 12, pp. 2947–2954, 2001.

[3] V. Cannillo, G. Pellacani, C. Leonelli, and A. Boccaccini, "Numerical modelling of the fracture behaviour of a glass matrix composite reinforced with alumina platelets," *Composites Part A: Applied Science and Manufacturing*, vol. 34, no. 1, pp. 43–51, 2003.

[4] V. Cannillo, C. Leonelli, T. Manfredini, M. Montorsi, and A. R. Boccaccini, "Computational simulations for the assessment of the mechanical properties of glass with controlled porosity," *Journal of Porous Materials*, vol. 10, no. 3, pp. 189–200, 2003.

[5] T. Liu, W. C. Tjiu, Y. Tong, C. He, S. S. Goh, and T.-S. Chung, "Morphology and fracture behavior of intercalated epoxy/clay nanocomposites," *Journal of applied polymer science*, vol. 94, no. 3, pp. 1236–1244, 2004.

[6] K. Wang, L. Chen, J. Wu, M. L. Toh, C. He, and A. F. Yee, "Epoxy nanocomposites with highly exfoliated clay: mechanical properties and fracture mechanisms," *Macromolecules*, vol. 38, no. 3, pp. 788–800, 2005.

[7] V. Cannillo, C. Leonelli, T. Manfredini, M. Montorsi, P. Veronesi, E. Minay, and A. Boccaccini, "Mechanical performance and fracture behaviour of glass–matrix composites reinforced with molybdenum particles," *Composites science and technology*, vol. 65, no. 7, pp. 1276–1283, 2005.

[8] F. Bondioli, V. Cannillo, E. Fabbri, and M. Messori, "Epoxy-silica nanocomposites: Preparation, experimental characterization, and modeling," *Journal of applied polymer science*, vol. 97, no. 6, pp. 2382–2386, 2005.

[9] B. Wetzel, P. Rosso, F. Haupert, and K. Friedrich, "Epoxy nanocomposites–fracture and toughening mechanisms," *Engineering fracture mechanics*, vol. 73, no. 16, pp. 2375–2398, 2006.

[10] N. Chawla, R. Sidhu, and V. Ganesh, "Three-dimensional visualization and microstructure-based modeling of deformation in particle-reinforced composites," *Acta materialia*, vol. 54, no. 6, pp. 1541–1548, 2006.

[11] S.-H. L. Kaiyang Zeng, "Fracture characteristics and indentation creep analysis of al2o3 – epoxy based nanocomposites," *Eng. Fracture Mechanics*, 2006.

[12] V. Cannillo, T. Manfredini, M. Montorsi, C. Siligardi, and A. Sola, "Microstructure-based modelling and experimental investigation of crack propagation in glass–alumina functionally graded materials," *Journal of the European Ceramic Society*, vol. 26, no. 15, pp. 3067–3073, 2006.

[13] Y. Dong, D. Bhattacharyya, and P. J. Hunter, "Experimental characterisation and object-oriented finite element modelling of polypropylene/organoclay nanocomposites," *Composites science and technology*, vol. 68, no. 14, pp. 2864–2875, 2008.

[14] H. Hu, L. Onyebueke, A. Abatan, *et al.*, "Characterizing and modeling mechanical properties of nanocomposites-review and evaluation," *Journal of Minerals and Materials Characterization and Engineering*, vol. 9, no. 04, p. 275, 2010.

[15] H. Wang, H. Zhou, R. Peng, and L. Mishnaevsky Jr, "Nanoreinforced polymer composites: 3d fem modeling with effective interface concept," *Composites Science and Technology*, vol. 71, no. 7, pp. 980–988, 2011.

[16] G. Dai and L. Mishnaevsky Jr, "Damage evolution in nanoclay-reinforced polymers: A three-dimensional computational study," *Composites Science and Technology*, 2012.

[17] N. K. Sharma, S. Pandit, and R. Vaish, "Microstructural modeling of ni-composites using object-oriented finite-element method," *ISRN Ceramics*, vol. 2012, 2012.

[18] G. Dieter, "Mechanical metallurgy, mcgracw-hill," 1976.

[19] A. K. Kaw, *Mechanics of composite materials*. CRC press, 2005.

[20] T. E. Twardowski, *Introduction to nanocomposite materials: properties, processing, characterization*. DEStech publications, Inc, 2007.

[21] M. H. Aliabadi and D. P. Rooke, *Numerical fracture mechanics*, vol. 8. Springer, 1991.

[22] N. Chawla, B. Patel, M. Koopman, K. Chawla, R. Saha, B. Patterson, E. Fuller, and S. Langer, "Microstructure-based simulation of thermomechanical behavior of composite materials by object-oriented finite element analysis," *Materials Characterization*, vol. 49, no. 5, pp. 395–407, 2002.

[23] A. C. Reid, R. C. Lua, R. E. García, and V. R. Coffman, "Modelling microstructures with oof2," *International Journal of Materials and Product Technology*, vol. 35, no. 3, pp. 361–373, 2009.

[24] S. R. Bakshi, R. R. Patel, and A. Agarwal, "Thermal conductivity of carbon nanotube reinforced aluminum composites: a multi-scale study using object oriented finite element method," *Computational Materials Science*, vol. 50, no. 2, pp. 419–428, 2010.

[25] Z. Hashin and S. Shtrikman, "A variational approach to the theory of the elastic behaviour of multiphase materials," *Journal of the Mechanics and Physics of Solids*, vol. 11, no. 2, pp. 127–140, 1963.

[26] P. Valavala and G. Odegard, "Modeling techniques for determination of mechanical properties of polymer nanocomposites," *Rev. Adv. Mater. Sci*, vol. 9, pp. 34–44, 2005.

[27] J. C. H. Affdl and J. L. Kardos, "The halpin-tsai equations: A review," *Polymer Engineering Science*, vol. 16, no. 5, pp. 344–352, 1976.

[28] J. C. H. Affdl and J. L. Kardos, "The halpin-tsai equations: A review," *Polymer Engineering Science*, vol. 16, no. 5, pp. 344–352, 1976.

[29] M. Avella, F. Bondioli, V. Cannillo, M. Errico, A. Ferrari, B. Focher, M. Malinconico, T. Manfredini, and M. Montorsi, "Preparation, characterisation and computational study of poly (ε-caprolactone) based nanocomposites," *Materials science and technology*, vol. 20, no. 10, pp. 1340–1344, 2004.

[30] V. Cannillo, F. Bondioli, L. Lusvarghi, M. Montorsi, M. Avella, M. Errico, and M. Malinconico, "Modeling of ceramic particles filled polymer–matrix nanocomposites," *Composites science and technology*, vol. 66, no. 7, pp. 1030–1037, 2006.

[31] Q. Zhang, G. Chen, G. Wu, Z. Xiu, and B. Luan, "Property characteristics of a alnp/al composite fabricated by squeeze casting technology," *Materials Letters*, vol. 57, no. 8, pp. 1453–1458, 2003.

[32] R. A. Schapery, "Thermal expansion coefficients of composite materials based on energy principles," *Journal of Composite Materials*, vol. 2, no. 3, pp. 380–404, 1968.

[33] "Google images." https://www.google.co.in/img. Accessed June 25, 2014.

[34] "Properties." http://www.matweb.com/. Accessed June 25, 2014.

[35] "howstuffworks." http://auto.howstuffworks.com/brakes. Accessed June 25, 2014.

[36] "Rusted sport brake." http://www.ctcms.nist.gov/ langer/oof2man/. Accessed June 25, 2014.

[37] "Composite materials." http://micro.magnet.fsu.edu/primer. Accessed May 25, 2014.

[38] "Wikipedia." https://www.google.co.in/img. Accessed Dec 4, 2013.